Transmittance study of a 1D superconductor-semiconductor photonic crystal

Alan Yuseth Herrera Flor

Degree work: Research project

Presented as partial requirement to qualify for the title of Physicist

Supervisor
Prof. Nelson Porras Montenegro

Universidad del Valle
Facultad de Ciencias Naturales y Exactas
Departamento de Física

February 2018

"En cualquier tarea se puede ganar o perder, lo importante es la nobleza de los recursos utilizados, lo importante es el tránsito. La dignidad con que recorrí el camino en la búsqueda del objetivo."

Marcelo Bielsa

"Ever tried. Ever failed. No matter. Try Again. Fail again. Fail better."

Samuel Beckett

Resumen

En este trabajo, usando el método de matriz transferencia (TMM) estudiamos la transmitancia de cristales fotónicos 1D formados por capas alternadas de un semiconductor (GaAs) y un superconductor de alta temperatura crítica ($HgBa_2Ca_2Cu_3O_{8+\delta}$) bajo cambios en la temperatura del sistema, presión hidrostática aplicada y espesor de las capas de los materiales. La fórmula de dispersión dependiente de la frecuencia para la permitividad dieléctrica se adoptó de acuerdo con el modelo de dos fluidos para describir la respuesta óptica del sistema superconductor. Se encontró que al aumentar el espesor de las capas superconductoras (semiconductoras) se produce un desplazamiento a valores más altos (más bajos) de la frecuencia de corte de transmitancia. Adicionalmente, esta frecuencia de corte se desplaza a valores más bajos con el aumento de la temperatura del sistema. Además, encontramos que el ancho de las brechas de banda fotónicas varía con la presión aplicada. La variación más notoria se presenta cerca a la región de 17 THz, donde se aprecia la aparición de un nuevo gap con el incremento de la presión. Calculamos además la estructura de bandas fotónica del sistema, basada en la ecuación trascendental derivada del TMM y del teorema de Bloch. Nos dimos cuenta de que las estructuras de banda son muy consistentes con los espectros de transmitancia. Esperamos que este trabajo se tenga en cuenta para el desarrollo de nuevas perspectivas en el diseño de nuevos dispositivos ópticos.

Abstract

In this work using the transfer matrix method (TMM) we study the transmittance of 1D photonic crystals made of alternated layers of a semiconductor (GaAs) and a high-T_c superconductor ($HgBa_2Ca_2Cu_3O_{8+\delta}$) under the effects of temperature, applied hydrostatic pressure and thickness of the layers. The frequency-dependent dispersion formula for dielectric permittivity was adopted according to the two-fluid model to describe the optical response of the superconducting system. We found that increasing the superconductor (semiconductor) layers thickness results in a shift to higher (lower) values of the transmittance cutoff frequency. Additionally, this cutoff frequency is shifted to lower values with the temperature increase. Furthermore, we found that the width of the photonic band gaps varies with the applied pressure. The most notorious variation is presented close 17 THz region, where a new gap appears with the pressure increase. We further calculated the photonic band structure of the system based on the transcendental equation derived from the TMM and Bloch theorem. We realized that the band structures are strongly consistent with the transmittance spectra. We hope this work may be taken into consideration for the development of new perspectives in the design of new optical devices.

Agradecimientos

Primero a mis mas grandes ídolos: Mis padres, Wilson Herrera y Claudia Patricia Flor, por absolutamente todo, ádemas de su esfuerzo y apoyo incondicional.

A mi abuela Carmelina: LA ABUELA, la que nunca se guardó nada y nada ha podido con ella. A mí otra abuela, i, que me dejó a mitad de camino y se convirtió en una motivación extra. Al igual que mi eterno Chiqui. A toda mi familia, en especial mis primos y mis tíos, por la alegría de cada domingo.

A mis mejores amigos, Diana y Diego, por las risas y placeres compartidos. A todo el M, por mantener viva esta amistad durante tanto tiempo. A mis compañeros de la universidad, que me han ayudado a lo largo de este camino, incluso a quienes han ido tomando diferentes rumbos.

A los diferentes profesores que también han hecho parte importante del camino, en especial al profe Nelson, que no se ha cansado de apoyarme, no solo con este proyecto, durante los últimos dos años. Igualmente agradezco a los jurados por el tiempo dedicado al análisis de este trabajo.

Contents

Resumen ii

Abstract iii

Acknowledgements iv

List of Figures vi

1 Introduction 1
- 1.1 Photonic Crystals . . . 1
  - 1.1.1 Superconducting Photonic Crystals . . . 2
- 1.2 Semiconducting material . . . 3
- 1.3 Superconducting material . . . 3

2 Theoretical framework 5
- 2.1 Transfer matrix method . . . 5
- 2.2 Semiconducting model . . . 9
- 2.3 Superconducting model . . . 9
  - 2.3.1 The two fluid model . . . 10
  - 2.3.2 Magnetic penetration depth . . . 14
  - 2.3.3 Pressure effect . . . 15

3 Results and discussions 17
- 3.1 Temperature dependence . . . 18
- 3.2 Layer thickness dependence . . . 20
  - 3.2.1 Superconducting thickness dependence . . . 20
  - 3.2.2 Semiconducting thickness dependence . . . 21
  - 3.2.3 Comparison between d_1 and d_2 . . . 22
- 3.3 Pressure dependence . . . 23

4 Conclusions 25

5 Outlook 26

6 Conference presentations and publications 27

Bibliography 29

List of Figures

1.1 Representation of a photonic crystal in one, two and three dimensions. Fig. taken from Ref. [1]. 2

2.1 Scattering of electromagnetic waves with TE polarization at an interface. 6
2.2 Structure of the PCs in this work 8
2.3 Schematic construction of the unit slab transfer matrix M_{us} 8
2.4 Schematic construction of the entire system transfer matrix M_t 9
2.5 Crystal structure of Hg1223. Red, blue, yellow, green and light blue spheres correspond to Hg, Ba, Ca, Cu and O, respectively. Reprinted from Ref. [30]. 10
2.6 Out-of-plane magnetic penetration depth for Hg-1223. Fig. taken from Ref. [39]. 15
2.7 Pressure dependence of T_c in Hg-1223. Reprinted from Ref. [30]. 16

3.1 Superconductor permittivity behavior as a function of the frequency for $T = 4, 50, 90$ and 120 K according with Eq. 2.36. 18
3.2 Transmittance spectra at different temperatures with Hg-1223 layer thickness $d_1 = 5$ μm, GaAs layer thickness $d_2 = 5$ μm, number of periods $N = 10$ and atmospheric pressure. 18
3.3 Cutoff frequency for transmittance at different temperatures with Hg-1223 layer thickness $d_1 = 5$ μm, GaAs layer thickness $d_2 = 5$ μm, number of periods $N = 10$ and atmospheric pressure. 19
3.4 Transmittance spectra of the structure with Hg-1223 layer thickness d_1 varied to be $1, 2, 5$ and 7 μm while semiconductor thickness d_2 is fixed at 5 μm. The temperature, pressure and number of periods are 90 K, 0 GPa and 10, respectively. 20
3.5 Transmittance spectra of the structure with GaAs layer thickness d_2 equal to $1, 2, 5$, and 7 μm while the superconductor thickness d_1 is fixed at 5 μm. The temperature, pressure and number of periods are 90 K, 0 GPa and 10, respectively. 21
3.6 Cutoff frequency for $d_1 = 1, 2, 5$ and 7 μm while d_2 was fixed at 5 μm. The temperature, pressure and number of periods are 90 K, 0 GPa and 10, respectively. 22
3.7 Cutoff frequency for $d_2 = 1, 2, 5$, and 7 μm while d_1 was fixed at 5 μm. The temperature, pressure and number of periods are 90 K, 0 GPa and 10, respectively. 23
3.8 Transmittance spectra for different pressures with $d_1 = 10$ μm and $d_2 = 5$ μm. The number of periods and temperature are 10 and 90 K, respectively. 24

Chapter 1

Introduction

1.1 Photonic Crystals

Many of the breakthroughs in our technology have resulted from a deeper understanding of the properties of materials. At present, there is a collection of synthetic materials with a huge range of mechanical properties, thanks to advances in metallurgy, ceramics and plastics. In the previous century, control over materials was extended to include its electrical properties. Advances in semiconductor physics have allowed us to tailor the conducting properties of certain materials, thereby initiating the transistor revolution in electronics. In the last few decades, a new frontier has opened up. The goal in this case is to control the optical properties of materials. An enormous range of technological developments would become possible if we could engineer materials that respond to light waves over a desired range of frequencies by perfectly reflecting them, or allowing them to propagate only in certain directions, or confining them within a specified volume [1]. Photonic crystals (PCs) are a particular type of these materials.

Since the publication of the works of Yablonovich [2] and John [3], PCs have been issue of investigation due to the tunability and mold of light passing through them. PCs are inhomogeneous artificial structures with periodically modulated dielectric constants in one, two, or three spatial directions, as shown in Fig. 1.1, and their spatial periods are in the order of a fraction of the optical wavelength [4].

PCs have attracted a lot of attention in the recent years due to their remarkable features and the possibility to be used in several applications. One of these important features is the inhibition of light propagation at some frequency ranges known as photonic band gaps (PBGs). In the photonic band gap region, the electromagnetic modes are absent. This phenomenon occurs due to the periodic variation of the refractive index at the

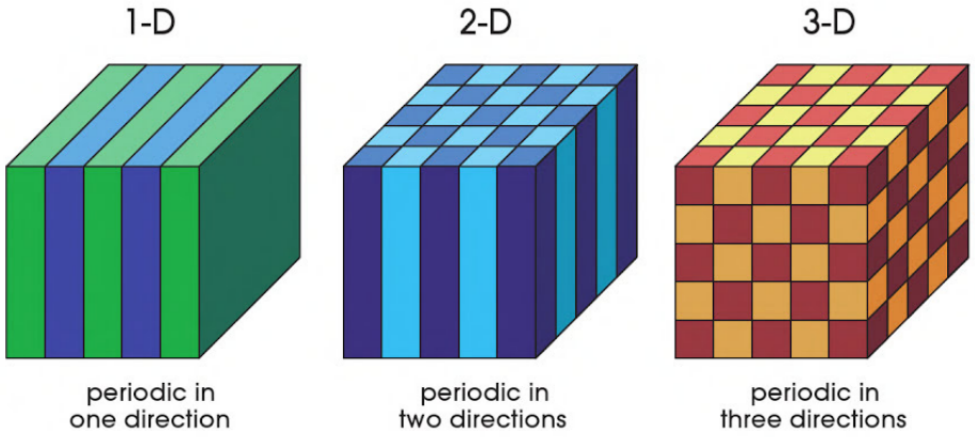


FIGURE 1.1: Representation of a photonic crystal in one, two and three dimensions. Fig. taken from Ref. [1].

crystal interface [5]. Among the most surprising effects of the existence of PBGs are the inhibition and the increase of spontaneous emission for atomic systems embedded in PCs [6, 7] as a consequence of externally controllable entangled atom-photon states, which originate when the atomic frequency is tuned in the vicinity of the band, leading to non-Markovian effects [8].

These materials represent an alternative and faster way of transmitting information, through the use of light as a carrier [9]. PCs can be the new raw material for making photonic circuits, this includes conduction channels such as optical waveguides [10] and logic components such as amplifiers, photonic transistors, etc... [11].

1.1.1 Superconducting Photonic Crystals

PCs composed of conventional materials like dielectrics or metals have been previously studied, but recently, superconducting PCs have attracted more attention due to two main advantages over the conventional material PC. Firstly, the reduction of damping in the electromagnetic waves that occur due to replacing PC metallic component by superconducting component [12]. Unlike conventional PCs, the PCs based on metallic and superconducting materials exhibit dispersive electromagnetic responses and high variability of PBG. Taking into account the negligible losses by dissipation below the critical temperature, the electromagnetic response of these materials, can be obtained assuming a non magnetic material and considering a frequency-dependent dielectric permittivity, which is well represented in the context of the two-fluid model [13]. The second one is that the dielectric function of the superconductor is mainly dependent on the London penetration depth, which is a function of the external temperature and external magnetic field as well [14, 15]. Due to these two characteristics, there has been great

interest in the study of PCs based on superconducting materials, both conventional and high critical temperature [16–20]. It has been found that the operating temperature can efficiently tune the cutoff frequency [4, 20], i.e. it has been found that the propagation of electromagnetic waves can be controlled to be prohibited in certain regions where their frequencies are less than the cutoff frequency value. For this reason, they can be used in applications such as high reflection mirrors, beam splitters and band pass filters [21–23].

1.2 Semiconducting material

Solids that are insulators at T=0, but whose energy gaps are of such size that thermal excitation can lead to observable conductivity at temperatures below the melting point, are known as semiconductors [24].

In the present work we use the GaAs compound as the semiconductor material to construct the PCs. Currently, this is one of the most used semiconductors. These two elements (Gallium and Arsenide) combine and form a III-V direct bandgap semiconductor with a zinc blende crystal structure. GaAs is used a lot of times for devices such as microwave frequency integrated circuits (ICs), monolithic microwave ICs, light-emitting diodes (LEDs), laser diodes and solar cells. GaAs is extremely useful in the field of high-speed circuits and a lot of systems incorporate ultrathin GaAs chips in the front end [25].

The effect of pressure and temperature on 1D air-GaAs PCs has already been studied in Ref. [26]. There it was found that the band structure is shifted to regions of higher frequencies and wider PBGs are obtained.

1.3 Superconducting material

Many metals, alloys, and intermetallic compounds undergo a phase transition at some (generally low) temperature, T_c, to a state having zero electrical resistance, a phenomenon which is called superconductivity and was discovered by Kamerlingh Onnes in 1911 [27]. Other fundamental characteristic associated with a superconductor is the exclusion of magnetic flux, discovered by W. Meissner and R. Ochsenfeld in 1933 (which is often known as the Meissner effect) [27].

In this work, for the superconducting material it is proposed to study the $HgBa_2Ca_2Cu_3O_{8+\delta}$ that is usually abbreviated as Hg-1223. This is a high temperature superconductor based on Mercury and is part of the cuprates superconductor family [28]. At present this is

the cuprate with the highest critical temperature (T_c) known [29, 30], reaching a T_c of up to 135 K.

Since a higher T_c implies higher operation temperatures, low cost, and better performance/reliability at a given temperature, these materials show great promise for practical applications. Despite this, still it has not been used as a component for superconducting PCs. One of the main features of this superconductor is the increase of its T_c by applying pressure, obtaining a T_c of up to 153 K at 21 GPa [30, 31] (hydrostatic pressure) and 164 K at 31 GPa (quasi-hydrostatic pressure) [32]. So far there are no reported studies on the effect of pressure in superconducting PCs.

In this project, we construct a one-dimensional PCs structure fabricated with alternated layers of semiconductor and superconductor, and study its transmittance response due to variations in: the system temperature, applied hydrostatic pressure and thickness of the layers, using the Transfer Matrix Method.

Chapter 2

Theoretical framework

We are going to deal with light propagation through a photonic crystal, which is a macroscopic situation, therefore we must make use of Maxwell's equations. In the project we work with the transfer matrix method, so a description of the method is presented below. After this, the two materials to be used in the PCs are modeled.

2.1 Transfer matrix method

First, we are going to construct the transfer matrix for an interface. By definition, in the case of the TE polarization the electric intensity $\vec{E}$ is parallel to the interface. In the notation of Fig. 2.1 we see that vector $\vec{E}$ has only one component, $\vec{E} = (0, E, 0)$ and vector $\vec{H}$ has two components, $\vec{H} = (H_x, 0, H_z)$. As shown in Fig. 2.1, each field contains components that propagate to the right (denoted by the superscript +) and components propagating to the left (denoted by the superscript –).

At the interface between two media, we need to satisfy certain boundary conditions, which states that the component of the electric intensity, parallel to the interface, is the same on both sides of the interface

$$E_1^+ + E_1^- = E_2^+ + E_2^-, \tag{2.1}$$

and the same holds for the intensity of the magnetic field

$$H_{1x}^+ + H_{1x}^- = H_{2x}^+ + H_{2x}^-. \tag{2.2}$$

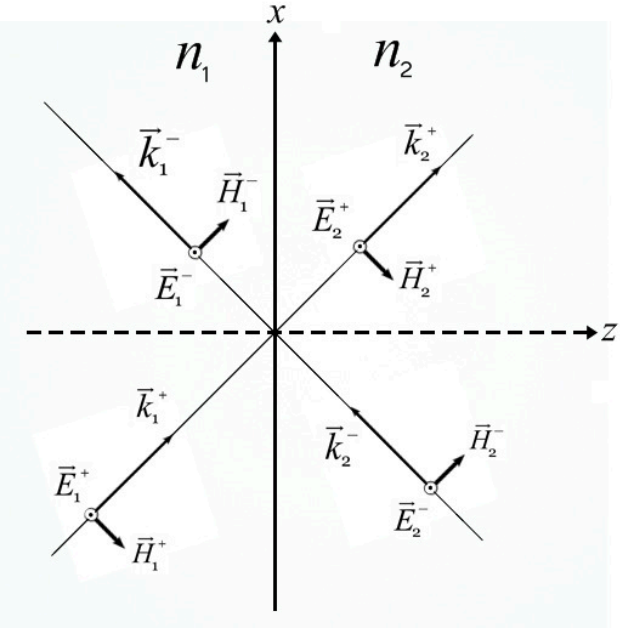


FIGURE 2.1: Scattering of electromagnetic waves with TE polarization at an interface.

We can express the magnetic field $\vec{H}$ in terms of $\vec{E}$ through Maxwells equations given by

$$\vec{k} \times \vec{E} = \frac{\mu\omega}{c}\vec{H}. \tag{2.3}$$

So for the medium 1 we have

$$\frac{\mu_1\omega}{c}H_{1x}^{+} = -k_{1z}E_1^{+}, \qquad \frac{\mu_1\omega}{c}H_{1x}^{-} = k_{1z}E_1^{-}, \tag{2.4}$$

here, k_{1z} is the z-component of the wave vector of the wave which propagates to the right. Inserting these in the boundary conditions (2.1) and (2.2) we can obtain.

$$-\frac{k_{1z}c}{\mu_1\omega}E_1^{+} + \frac{k_{1z}c}{\mu_1\omega}E_1^{-} = -\frac{k_{2z}c}{\mu_2\omega}E_2^{+} + \frac{k_{2z}c}{\mu_2\omega}E_2^{-}. \tag{2.5}$$

It is solved in the same way for medium 2. This system can be written in matrix form as:

$$\begin{pmatrix} 1 & 1 \\ -\frac{k_{1z}}{\mu_1} & +\frac{k_{1z}}{\mu_1} \end{pmatrix} \begin{pmatrix} E_1^{+} \\ E_1^{-} \end{pmatrix} = \begin{pmatrix} 1 & 1 \\ -\frac{k_{2z}}{\mu_2} & +\frac{k_{2z}}{\mu_2} \end{pmatrix} \begin{pmatrix} E_2^{+} \\ E_2^{-} \end{pmatrix}, \tag{2.6}$$

which express the electric field on one side of the interface in terms of the electric field on the other side. From equation (2.6) we can obtain a relation between the electric fields on opposite sides of the interface in the following way:

$$\begin{pmatrix} E_2^+ \\ E_2^- \end{pmatrix} = M_{12} \begin{pmatrix} E_1^+ \\ E_1^- \end{pmatrix}, \tag{2.7}$$

with the transfer matrix M_{12} to go from medium 1 to medium 2 given by

$$M_{12} = \frac{1}{2} \begin{pmatrix} 1 + \frac{\mu_2}{\mu_1}\frac{k_{1z}}{k_{2z}} & 1 - \frac{\mu_2}{\mu_1}\frac{k_{1z}}{k_{2z}} \\ 1 - \frac{\mu_2}{\mu_1}\frac{k_{1z}}{k_{2z}} & 1 + \frac{\mu_2}{\mu_1}\frac{k_{1z}}{k_{2z}} \end{pmatrix}. \tag{2.8}$$

Considering normal incidence ($k_{1z} = k_1$ and $k_{2z} = k_2$), non-magnetic materials ($\mu_1 = \mu_0 = \mu_2$) and taking into account that k is given by $k_i = \frac{w}{c} n_i$ (i for medium 1 or 2), the transfer matrix for the interface can be written as:

$$M_{12} = \frac{1}{2} \begin{pmatrix} 1 + \frac{n_1}{n_2} & 1 - \frac{n_1}{n_2} \\ 1 - \frac{n_1}{n_2} & 1 + \frac{n_1}{n_2} \end{pmatrix}. \tag{2.9}$$

Now for propagation inside a homogenous medium between two interfaces, we have the diagonal propagation matrix P_i given by [33]

$$P_i = \begin{pmatrix} e^{ik_i d_i} & 0 \\ 0 & e^{-ik_i d_i} \end{pmatrix}, \tag{2.10}$$

where k_i is the wave vector inside the medium and d_i is the thickness of the layer between the two interfaces.

The geometry of the system is shown in Fig. 2.2. This structure is composed of two materials; the first is the superconductor with thickness d_1 and the second is the semiconductor with thickness d_2.

Now, with these two matrices M_{12} and P_i, we can construct a matrix for a unit slab (M_{us}) in the following way: Starting inside the superconductor medium 1, we apply the matrix P_1 that propagates the wave through medium 1, then use the matrix M_{12} to go from medium 1 to medium 2, now we must propagate the wave along medium 2 with P_2 and to return again to our starting point i.e. medium 1, we use M_{21} to go from medium 2 to medium 1, such as is in the outline of the Fig. 2.3.

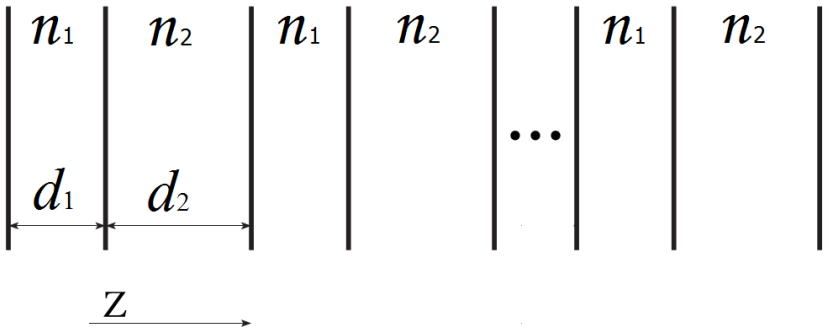


FIGURE 2.2: Structure of the PCs in this work

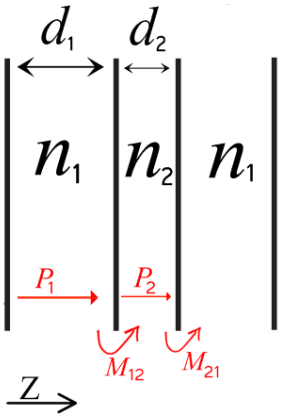


FIGURE 2.3: Schematic construction of the unit slab transfer matrix M_{us}

$$M_{us} = M_{21} \cdot P_2 \cdot M_{12} \cdot P_1. \tag{2.11}$$

Hence, if we want to build a structure of the form $(AB)^N$, where A is the superconductor and B the semiconductor, we assume that the crystal is embedded in air, which we call medium 0, and we start from this medium 0. We use the matrix M_{01} to go from the air to the superconductor, already located in the superconductor we can use the matrix of the unit slab that we built previously and we will reproduce it $N-1$ times. At the end of this product, we go out again in the medium 1 superconductor, then we propagate through this medium with P_1, we transfer to medium 2 with M_{12}, we propagate through medium 2, and to go back into the air we use the matrix M_{20}. All this can be seen easier in the scheme of Fig. 2.4.

$$M_t = M_{20} \cdot P_2 \cdot M_{12} \cdot P_1 \cdot (M_{us})^{N-1} \cdot M_{01}. \tag{2.12}$$

Then the transmission coefficient is calculated [33] as

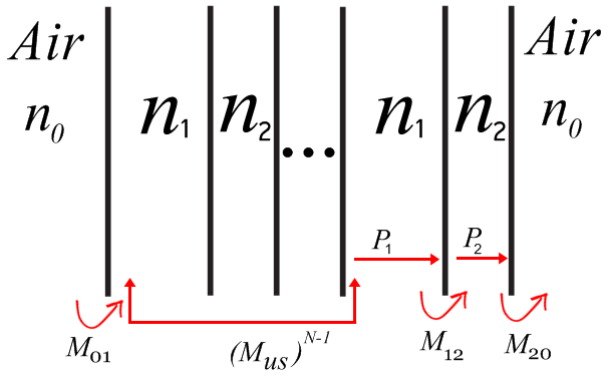


FIGURE 2.4: Schematic construction of the entire system transfer matrix M_t

$$T = \frac{1}{|M_{t_{22}}|^2}. \tag{2.13}$$

2.2 Semiconducting model

To describe the optical response of the semiconductor layer we follow the works by Samara [34] and Elabsy [35] on the GaAs dielectric constant, which have been fitted [26, 36] as function of pressure and temperature in the following way:

$$\epsilon_r(P,T) = \left(\epsilon_0 + Ae^{T/T_0}\right) e^{-\alpha P}, \tag{2.14}$$

where $\epsilon_0 = 12.446$, $A = 0.21125$, $T_0 = 240.7$ K, and $\alpha = 0.0173$ GPa^{-1}. After this, the refractive index can be calculated as $\sqrt{\epsilon_r}$. While for the thickness of the layer

$$d_2(P) = d_0[1 - (S_{11} + 2S12)P], \tag{2.15}$$

being d_0 the original thickness of the layer, and $S_{11} = 1.16 \times 10^{-2}$ GPa^{-1}, and $S_{12} = -3.7 \times 10^{-3}$ GPa $^{-1}$ are the elastic constants of the GaAs [37].

2.3 Superconducting model

On the other hand to describe the optical response of the superconducting material we consider the two fluid model [13, 14].

Given the high anisotropy of the superconducting material, shown in Fig. 2.5, we only consider perpendicular propagation to the c-axis of the Hg-1223.

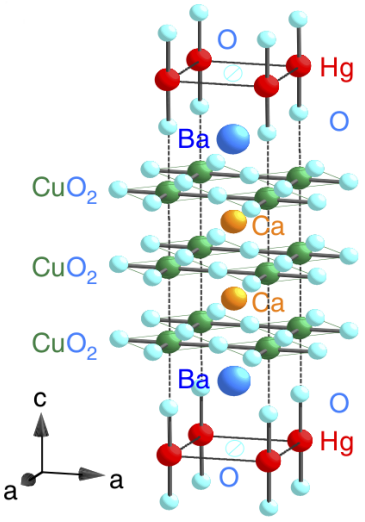


FIGURE 2.5: Crystal structure of Hg1223. Red, blue, yellow, green and light blue spheres correspond to Hg, Ba, Ca, Cu and O, respectively. Reprinted from Ref. [30].

2.3.1 The two fluid model

To describe the response of electromagnetic waves of a non-magnetic superconductor at non-zero temperature we use the two-fluid model. According to this two fluid model, the electrons in the superconductor occupy one of two states: superconducting state or normal state. In a general two-fluid model, one assumes that the total electron density n can be divided into two parts: the density of superconducting electrons is n_s, and that of normal electrons is n_n, and they have different relaxation times[1] τ_s, and τ_n.

The normal electrons, with number density n_n behave in exactly the same way as the free electrons in a normal metal. They are accelerated by an electric field $\vec{E}$, but are frequently scattered by impurities and defects in the ion lattice and by thermal vibrations of the lattice. Interspersed with the normal electrons are the superconducting electrons, which form a fluid with number density n_s. The superconducting electrons are not scattered by impurities, defects or thermal vibrations, so they are freely accelerated by an electric field. Assuming a Drude model for both fluids in the following way

$$m\frac{dv_i}{dt} = eE - \frac{mv_i}{\tau_i}. \tag{2.16}$$

So long as we are interested only in the linear response of the superconductor, it is very convenient to Fourier analyze the applied electric field and to treat the response to each

[1]The relaxation time is the mean time between scattering events for the electrons

frequency separately. According to Eq. 2.16, the ac response of either parallel channel ($i = n,\ s$) to a field Ee^{jwt} is described by a complex conductivity

$$\sigma_i(\omega) \equiv \sigma_{1i}(\omega) - j\sigma_{2i}(\omega) = \frac{n_i e^2 \tau_i/m}{1 + j\omega\tau_i}, \tag{2.17}$$

whose real and imaginary parts are:

$$\sigma_{1i}(\omega) = \frac{\sigma_{0i}}{1 + \omega^2\tau_i^2}, \tag{2.18}$$

$$\sigma_{2i}(\omega) = \frac{\sigma_{0i}\omega\tau_i}{1 + \omega^2\tau_i^2}, \tag{2.19}$$

where $\sigma_{0i} \equiv n_i e^2\tau_i/m$. If we now describe the superconducting electrons by letting τ_s increase continuously to ∞, we see that the $\sigma_{1s}(\omega)$ curve becomes higher and higher at $\omega = 0$ but cuts off at a lower and lower frequency, retaining a constant area under the curve. Eventually, it shrinks to a δ function $\sigma_{1s}(\omega) = (\pi/2)(n_s e^2/m)\delta(\omega)$, which can be confirmed by an elementary integration of $\int \sigma_{1s}(\omega)d\omega$ over positive frequencies. In this same limiting process, $\sigma_{2s}(\omega)$ approaches the limit $n_s e^2/m\omega$, which is equivalent to the first London equation [14]. Therefore, the combined response of the two fluids to an electric field is given by

$$\begin{aligned}\sigma = \sigma_n + \sigma_s &= (\sigma_{1s} - j\sigma_{2s}) + (\sigma_{1n} - j\sigma_{2n}) = (\sigma_{1s} + \sigma_{1n}) - j(\sigma_{2s} + \sigma_{2n}) \\ &= \left(\frac{\pi}{2}\frac{n_s e^2}{m}\delta(\omega) + \frac{n_n e^2\tau_n/m}{1 + \omega^2\tau_n^2}\right) - j\left(\frac{n_s e^2}{m\omega} + \frac{n_n e^2\tau_n^2\omega/m}{1 + \omega^2\tau_n^2}\right)\end{aligned} \tag{2.20}$$

From now on, τ_n will be just τ unless it's indicated in the text. Reorganizing some terms, the most general complex conductivity is written as

$$\sigma = \left(\frac{e^2}{m}\right)\left[\frac{n_n\tau(1 - j\tau\omega)}{1 + \omega^2\tau^2} - j\frac{n_s}{\omega} + \frac{\pi}{2}n_s\delta(\omega)\right]. \tag{2.21}$$

For non-zero frequency, the last term is dropped and Eq. 2.21 reduces to

$$\sigma = \left(\frac{e^2}{m}\right)\left[\frac{n_n\tau(1 - j\tau\omega)}{1 + \omega^2\tau^2} - j\frac{n_s}{\omega}\right]. \tag{2.22}$$

Since this treatment applies only to frequencies below the superconducting gap Δ, given that for frequencies of the incident wave above the gap, the superconducting state disappears [14] and we are interested in a non-dissipative superlattice, it is usually possible to assume that frequencies are also low enough so that $\omega\tau \ll 1$ (condition 1) [13, 38]. After this, Eq. 2.22 reduces to

$$\sigma = \frac{e^2}{m}\left[n_n\tau(1 - j\tau\omega) - jn_s/\omega\right] \tag{2.23}$$

When $n_n\tau \ll jn_s/\omega$ (condition 2) [13, 38] is satisfied, the complex conductivity [Eq. 2.23] approximates to imaginary and the desired case of non-dissipative superlattice is obtained.

$$\sigma(\omega) \approxeq -je^2n_s/m\omega. \tag{2.24}$$

Condition 1 and Condition 2 enable the conductivity to be simply expressed in terms of the magnetic penetration depth λ_L, since $m/\mu_0 n_s e^2 = \lambda_L^2$ [13]. In superconductors, this magnetic penetration depth, also called London penetration depth characterizes the distance to which a magnetic field penetrates into a superconductor.

$$\sigma(\omega) \approxeq -j/\mu_0\omega\lambda_L^2 \tag{2.25}$$

In the superconductor layer with no external source current and charge, the Maxwells equations becomes

$$\nabla \times \vec{E} = -\frac{\partial \vec{B}}{\partial t} \tag{2.26}$$

$$\nabla \cdot \vec{E} = 0 \tag{2.27}$$

$$\nabla \cdot \vec{B} = 0 \tag{2.28}$$

$$\nabla \times \vec{B} = \sigma\mu_0\vec{E} + \epsilon_0\mu_0\frac{\partial \vec{E}}{\partial t} \tag{2.29}$$

Taking the curl of Eq. 2.29, and using Eqs. 2.26 and 2.28 we have:

$$\nabla \times (\nabla \times \vec{B}) = \nabla(\nabla \cdot \vec{B}) - \nabla^2 \vec{B} = -\nabla^2 \vec{B} = \sigma\mu_0 \nabla \times \vec{E} + \epsilon_0\mu_0 \frac{\partial(\nabla \times \vec{E})}{\partial t} \tag{2.30}$$

$$\nabla^2 \vec{B} - \sigma\mu_0 \frac{\partial \vec{B}}{\partial t} - \epsilon_0\mu_0 \frac{\partial^2 \vec{B}}{\partial t^2} = 0. \tag{2.31}$$

Using the convention $\vec{B} \propto e^{j(\omega t - \vec{k}\cdot\vec{r})}$, the action of the differential operators on the field is given by: $\nabla^2 \vec{B} = -k^2 \vec{B}$, $\partial \vec{B}/\partial t = j\omega \vec{B}$, and $\partial^2 \vec{B}/\partial t^2 = -\omega^2 \vec{B}$. Therefore Eq. 2.31 takes the form

$$-k^2 - j\mu_0\sigma\omega + \omega^2\epsilon_0\mu_0 = 0 \tag{2.32}$$

To finally get the following dispersion relation

$$k^2 = \frac{\omega^2}{c^2}\left(1 - \frac{j\sigma}{\epsilon_0\omega}\right), \tag{2.33}$$

which according to $k^2 = \frac{\omega^2}{c^2} n^2(\omega)$, gives us the following expression for the superconductor refractive index

$$n^2(\omega) = 1 - \frac{j\sigma}{\epsilon_0\omega}. \tag{2.34}$$

Going back to Eq. 2.25 for the conductivity of the superconductor, the final expression for the refractive index can be written as:

$$n(\omega) = \sqrt{1 - \frac{c^2}{\omega^2\lambda_L^2}}, \tag{2.35}$$

from $n(\omega) = \sqrt{\epsilon_r}$ we can obtain the relative permittivity of the superconducting material:

$$\epsilon_r = 1 - \frac{\omega_{sp}^2}{\omega^2}, \tag{2.36}$$

where $\omega_{sp} = c/\lambda_L$.

2.3.2 Magnetic penetration depth

As mentioned before, the magnetic penetration depth characterizes the magnetic field penetrating distance into the superconductor. To perform the calculations with the refractive index given by Eq. 2.35 we need to find a λ_L expression for the superconductor.

Generally, high temperature superconductors are highly anisotropic, so its different properties depends on the direction of the incoming electromagnetic radiation. One of this properties is justly the magnetic penetration depth, which depends on the magnetic field direction. For a magnetic field parallel to the c-axis ($H \parallel c$) of the superconductor, it is necessary to use the in-plane magnetic penetration depth, or λ_{ab}. Conversely, when the magnetic field is parallel to the ab-plane ($H \parallel ab$) of the material, the corresponding λ is the out-of-plane magnetic penetration depth, or λ_c.

Remembering that the propagation (in the z axis) in the PC is perpedicular to the c-axis of the superconducting material we have two options: Magnetic field parallel to the c-axis (in the x direction) or magnetic field parallel to the ab-plane (in the y direction).

For the in-plane λ_{ab} in the Hg-1223 we can make use of Ginzburg-Landau [27] theory to obtain an explicit expression which works very well for T near T_c and has been experimentally proved [39]. But this case would imply that the electric field is parallel to the ab-plane, i.e. parallel to the CuO_2 planes of the cuprate superconductor. This field could influence the creation of surface plasmons in these metallic planes, and that would be an extra problem to take into account in our calculations.

To avoid this trouble, we took $\lambda_L = \lambda_c$, i.e. magnetic field parallel to the ab-plane and electric field perpendicular to the CuO_2 planes, which guarantees that surface plasmons will no longer be produced. Unfortunately, there is no theoretical expression for this out-of-plane magnetic penetration depth in the Hg-1223. But, we found a complete set of measurements from Prof. Panagopoulos [39] for λ_c as a function of temperature from ~ 0 K to ~ 130 K. Below, in Fig. 2.6 are presented the mentioned measurements.

The corresponding fit to the data points was performed and the following relation was obtained:

$$\lambda_L(T) = \frac{\lambda_0}{\sqrt[3]{1 - \left(\frac{T}{T_c}\right)^3}}, \tag{2.37}$$

where $\lambda_0 = 6100$ nm is the out-of-plane magnetic penetration depth at zero temperature. This model is similar to other models used in superconductors (Gorter-Casimir [21], Ginzburg-Landau [40]) where λ_L is a function of a radical in the denominator which

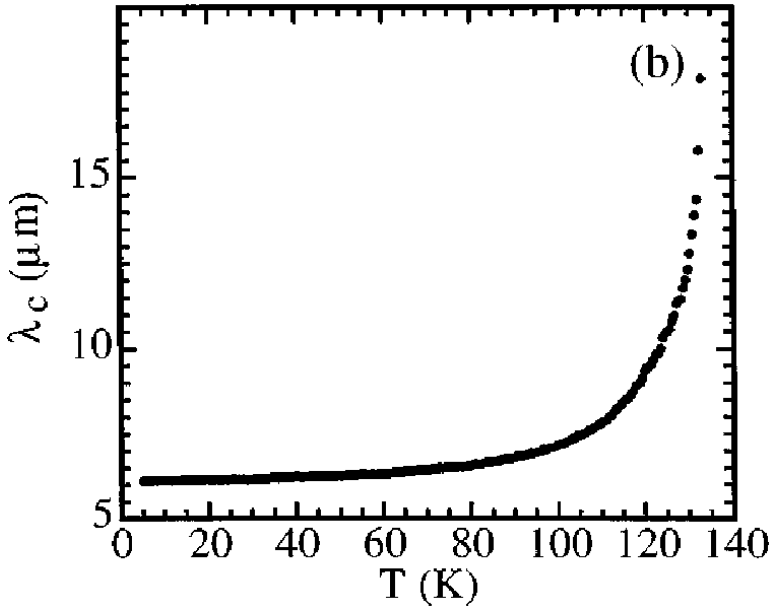


FIGURE 2.6: Out-of-plane magnetic penetration depth for Hg-1223. Fig. taken from Ref. [39].

contains a term of the form $(1 - T/T_c)$. Using λ_L from Eq. 2.37 in the refractive index equation (2.35) we obtained the final expression for our transfer matrix calculations.

2.3.3 Pressure effect

As introduced before, by including hydrostatic pressure variations in the Hg-1223, the critical temperature is modified [30, 31], and therefore also the λ_L. Likewise, the thickness of the superconducting layer is modified according to its compressibility constant $\kappa_a = 2.57 \times 10^3$ GPa^{-1} [41]. Here we assume that λ_0 keeps constant.

There are several ways to define T_c from resistivity measurements $\rho(T)$. In the literature, T_c has been defined either as (1) the temperature where $\rho(T)$ shows a negative deviation from the normal-state T-dependence, as defined by a rising edge in $d\rho(T)/dT$ and is termed T_c *onset*, or as (2) the temperature at which the resistivity drop is steepest [where $d\rho(T)/dT$ is largest (peaked)], and is termed T_c *mid* [31]. Another way to define T_c is the temperature where the resistivity is zero, T_c *zero*, and where the graph of $d\rho(T)/dT$ begins to be zero and remains constant at lower T (See Fig. 3 (b) in [31]).

This latter is the most reliable measure of the critical temperature, because guarantees the essential requirement for superconductivity that is the critical temperature needed to obtain zero resistivity. The other datapoints: T_c *onset*, and T_c *mid* does not necessarily prove the occurrence of superconductivity.

The relationship between the critical temperature and pressure increase can be seen in Fig. 2.7, where T_c is presented as function of pressure for the Hg-1223.

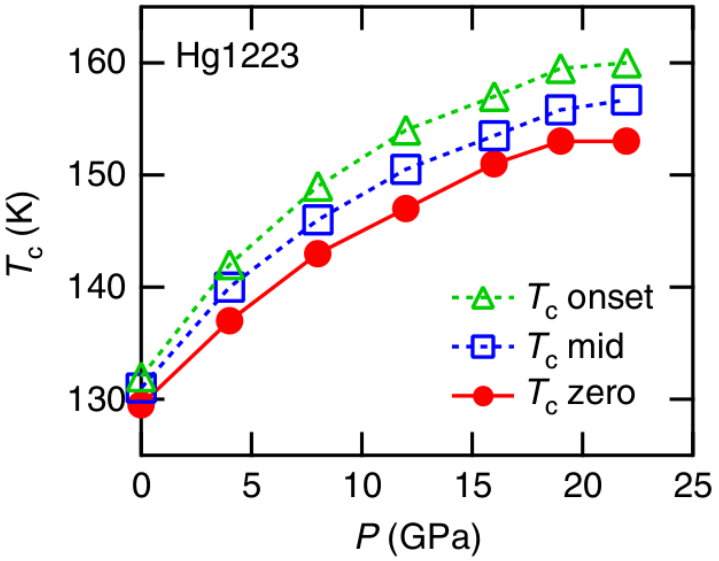


FIGURE 2.7: Pressure dependence of T_c in Hg-1223. Reprinted from Ref. [30].

Therefore, we are taking T_c as T_c zero in our calculations, because this guarantees that the contribution of the fraction of normal electrons is zero in the working regions ($T = 0$ to 130 K). This is in agreement with the fact that T_c *zero* is the lowest from the three definitions of T_c.

The adjustment of the critical temperature due to the pressure can be made in the following way:

$$T_c(P) = q_1 + q_2 P + q_3 P^2, \tag{2.38}$$

where $q_1 = 134$ K, $q_2 = 2.009$ K/GPa, and $q_3 = -4.194 \times 10^{-2}$ K/GPa^2 are simply fitting constants to the data from Fig. 2.7.

Chapter 3

Results and discussions

As it was established in the previous chapters, in the calculation of the transmittance for 1D photonic crystals, the transfer matrix method was used. In our simulations, we considered the superconductor material to be Hg-1223, so $T_c = 134$ K [29], $\lambda_0 = 6100$ nm [39].

It is worth to mention that superconductor materials have a characteristic superconducting energy gap Δ, that can be defined as the energy difference between the ground state of the superconductor and the energy of the lowest quasiparticle excitation [14]. So, if we send frequencies (energy) beyond the superconducting energy gap, the superconducting state can dissapear and therefore the two fluid model would be useless. This clarification is done because apparently most of the works [4, 15, 20, 42, 43] carried up to now in superconducting photonic crystals have not take this condition into account and their operational frequencies are beyond the superconducting gap Δ.

That said, in our work we calculated the relation between the transmittance and the frequency in the THz region, under the superconducting energy gap ($\sim$24 THz) [44] and assumed the case of normal incidence.

To start the analysis, we present below in Fig. 3.1 the dielectric constant ϵ_r behavior as a function of the frequency for different temperatures.

The superconductor plasma frequency $\omega_{sp} = c/\lambda_L$ in Eq. 2.36 presents a similar behavior to that of the plasma frequency in Drude model for metals, that is, when the frequency $\omega > \omega_{sp}$, ϵ_r of the superconductor is positive and the electromagnetic waves can propagate in the superconductor. Conversely, for $\omega < \omega_{sp}$ occurs that the electromagnetic waves propagation is prohibited in the superconductor, hence it will be an evanescent wave.

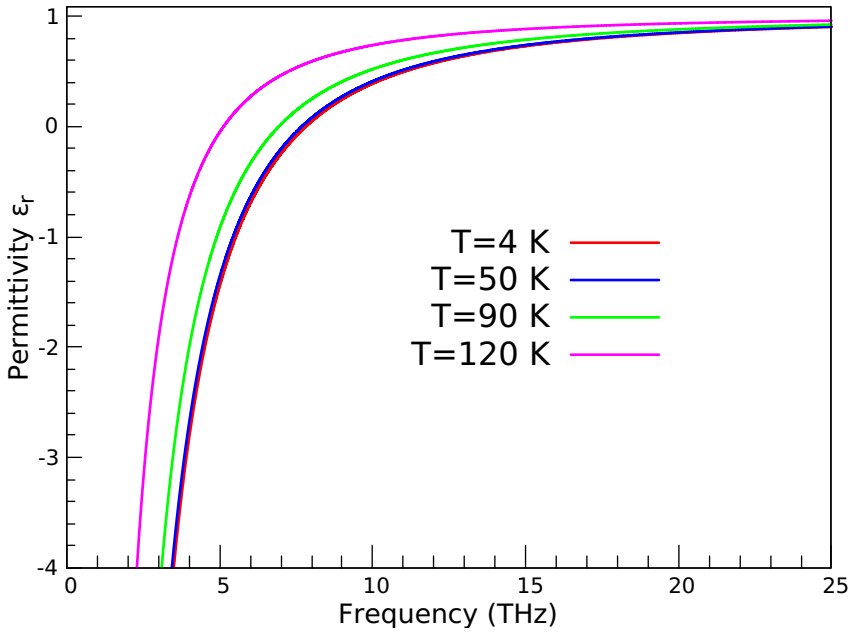


FIGURE 3.1: Superconductor permittivity behavior as a function of the frequency for $T = 4, 50, 90$ and 120 K according with Eq. 2.36.

3.1 Temperature dependence

The transmittance spectra of our structure when the system temperature is varied is shown in Fig. 3.3.

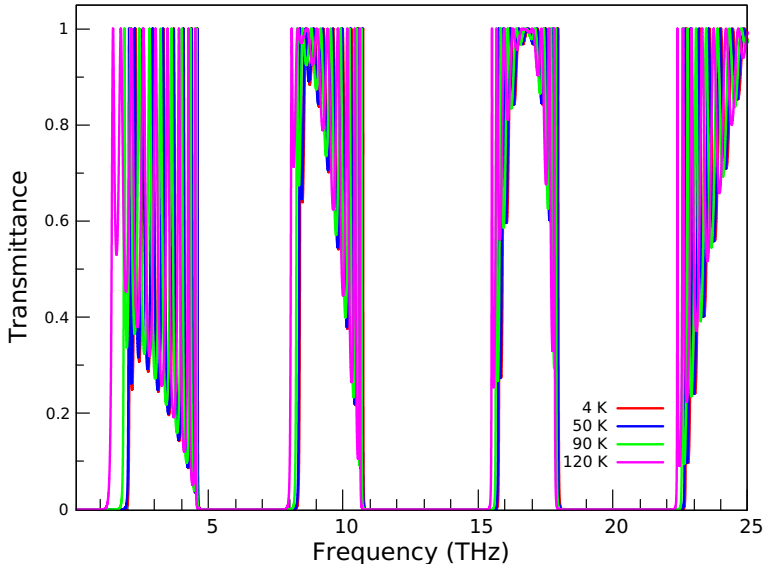


FIGURE 3.2: Transmittance spectra at different temperatures with Hg-1223 layer thickness $d_1 = 5$ μm, GaAs layer thickness $d_2 = 5$ μm, number of periods $N = 10$ and atmospheric pressure.

We considered that the number of periods N is equal to 10, the thickness of the superconductor and semiconductor layers were $d_1 = 5$ μm and $d_2 = 5$ μm respectively, and

the considered pressure was the atmospheric one. As the system temperature goes from T=4 K to 120 K the spectra present no noticeable variations. However, it is observed a small decrease in the cutoff frequency. This can be better noted in Fig. 3.3, where region of the cutoff frequencies has been zoomed.

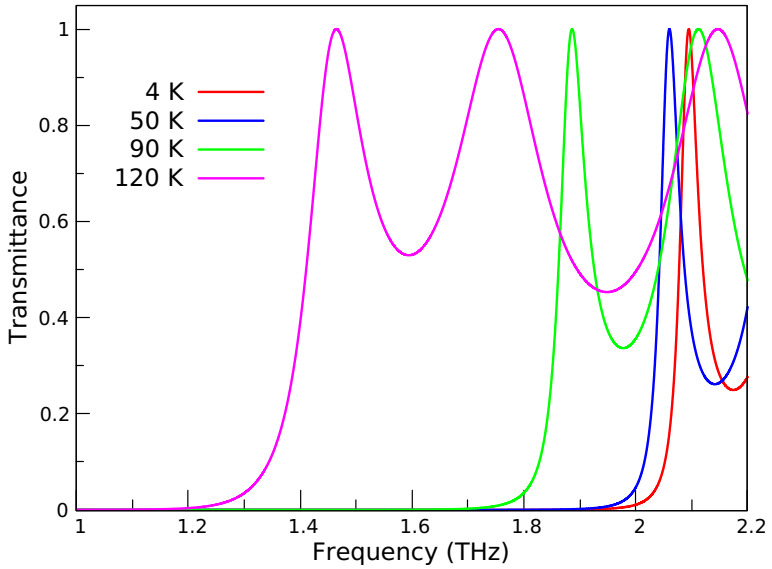


FIGURE 3.3: Cutoff frequency for transmittance at different temperatures with Hg-1223 layer thickness $d_1 = 5$ μm, GaAs layer thickness $d_2 = 5$ μm, number of periods $N = 10$ and atmospheric pressure.

Here the cutoff frequency varies from $\sim$ 2.1 THz at 4 K to $\sim$ 1.4 THz at 120 K. This behavior is in agreement with previous works [4, 20, 23] that have been presented so far, despite the difference in the operational frequencies used.

These results indicate that the propagation of the electromagnetic waves can be forbidden through the PC when their frequency is less than the cutoff frequency. It is worth to notice than this cutoff frequency differs from the superconductor plasma frequency ω_{sp}. For $T = 4$ K, the difference between ω_{sp} and the cutoff frequency is about 47 THz, while for $T = 120$ K, the difference is close to the 31 THz. This occurs due to the periodic structure of the PC, which allows some of the frequencies below ω_{sp} to transmit after several reflections in the different layers. For understanding these results, we can consider Fig. 3.1. For $\omega > 15$ THz, the dielectric constants values tend to one and no noticeable changes are observed with the temperature; while for $\omega < 15$ THz, the dielectric constant starts to vary with the temperature, taking values from 0.4 to -0.7 approximately at 4 and 120 K, respectively for $\omega = 6$ THz. As the dielectric constant increases with the frequency, the transmission should suffer a shifting to higher frequencies, result which is in agreement with the electromagnetic variational principle [1].

3.2 Layer thickness dependence

We have also studied the behavior of the transmittance spectra at different thicknesses of the superconductor and semiconductor layers. We examined the superconductor (semiconductor) thickness dependence fixing d_2 (d_1). In both cases, we used $T = 90$ K, $N = 10$ and $P = 0$ GPa.

3.2.1 Superconducting thickness dependence

Below, in Fig. 3.4 is presented the superconductor thickness dependence on the transmittance spectra of the structure.

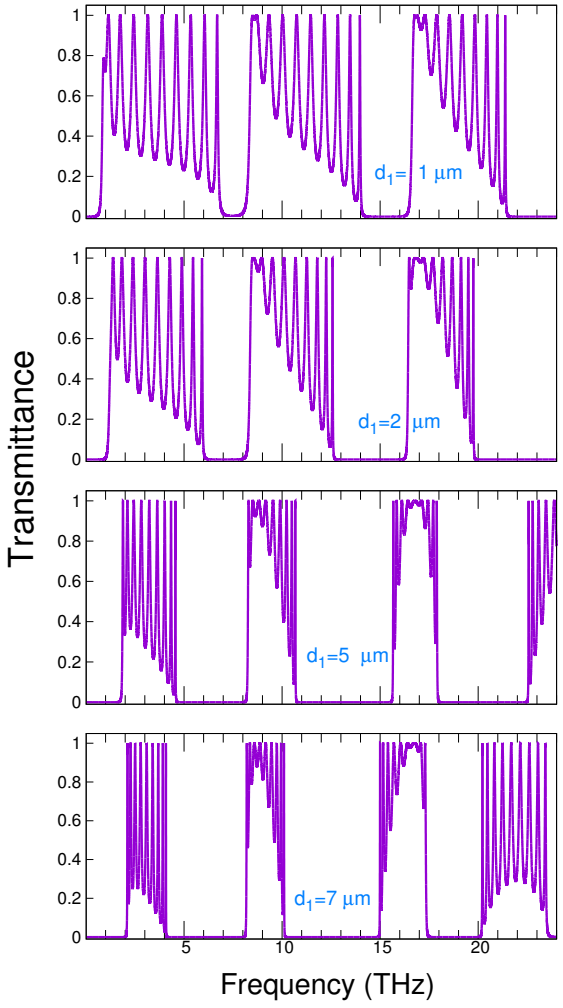


FIGURE 3.4: Transmittance spectra of the structure with Hg-1223 layer thickness d_1 varied to be $1, 2, 5$ and 7 μm while semiconductor thickness d_2 is fixed at 5 μm. The temperature, pressure and number of periods are 90 K, 0 GPa and 10, respectively.

We note in Fig. 3.4 when the thickness of the GaAs layers was fixed at $d_2 = 5$ μm and the thickness of the Hg-1223 layers was varied ($d_1 = 1, 2, 5$ and 7 μm), the cutoff frequency

shifted a small amount to higher values. This means that the cutoff frequency increased by increasing the superconductor layer thickness. Furthermore, as the thickness d_1 increases, the gaps shifts to lower frequency regions. The oscillations are further joined and a new gap is observed in the same region ($0 - 24$ THz) for the larger thickness ($d_1 = 7$ μm). Just as for the temperature case, the cutoff frequency dependence with the superconductor layer thickness is in agreement with previous works presented so far [4, 20, 23], even some of them are not presented in the proper frequency range.

3.2.2 Semiconducting thickness dependence

Fig. 3.5 shows the transmittance dependence with semiconductor thickness variation.

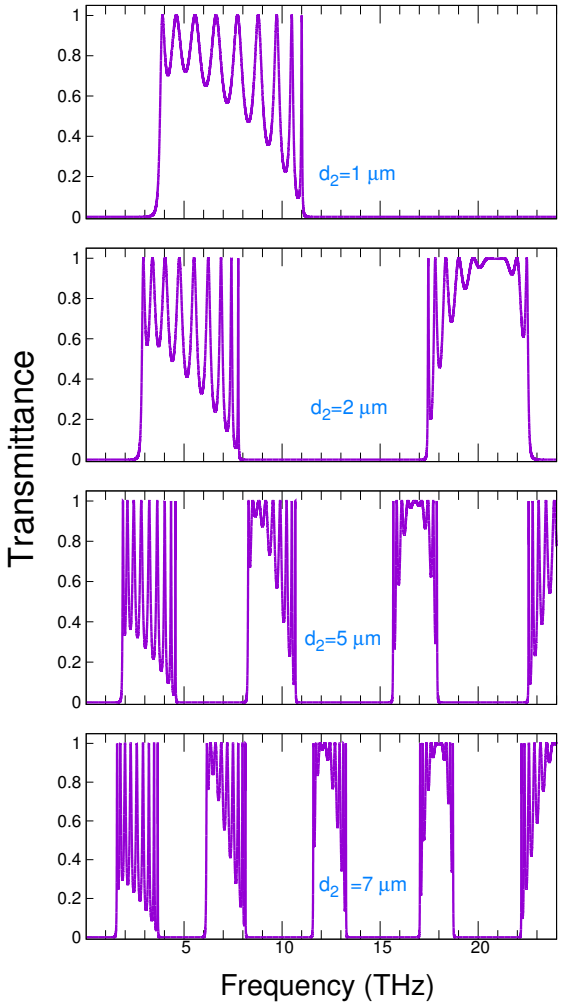


FIGURE 3.5: Transmittance spectra of the structure with GaAs layer thickness d_2 equal to $1, 2, 5$, and 7 μm while the superconductor thickness d_1 is fixed at 5 μm. The temperature, pressure and number of periods are 90 K, 0 GPa and 10, respectively.

When the thickness of the Hg-1223 layer was fixed at $d_1 = 5$ μm and the thickness of GaAs layer was varied ($d_2 =$ 1,2, 5 and 7 μm), the cutoff frequency decreased by

increasing the semiconductor layer thickness. Moreover, when the semiconductor layer thickness is increased, several new gaps appear for the larger thicknesses ($d_2 = 5$, 7 μm) in the same region ($0 - 24$ THz), unlike increasing the superconductor layer which only produced the appearance of one new gap when the thickness was the largest ($d_1 = 7$ μm).

3.2.3 Comparison between d_1 and d_2

To compare the two previous responses and how the cutoff frequency varies with changes in the thicknesses of the layers in the structure we made a zoom close to the cutoff frequencies for similar thicknesses and compared both variations.

In the first figure, Fig. 3.6, we fixed d_2 at 5 μm and d_1 was varied; and in the same way in the second figure, Fig. 3.7, we fixed d_1 at 5 μm and d_2 was varied.

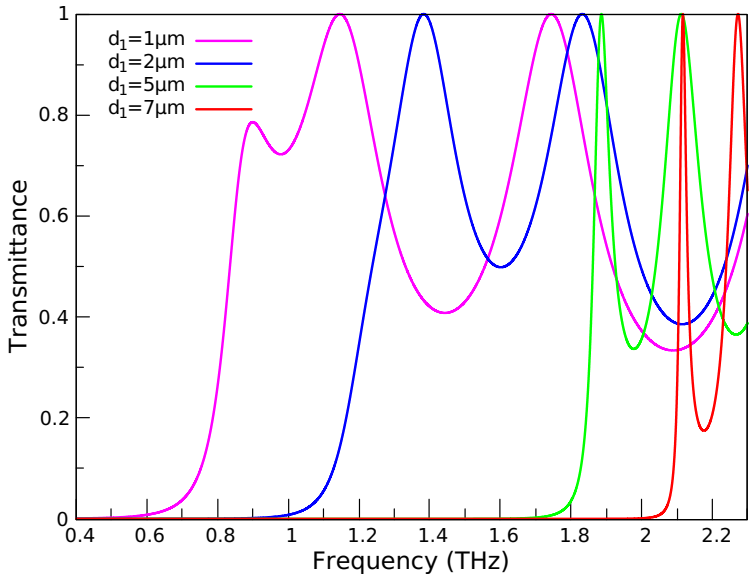


FIGURE 3.6: Cutoff frequency for $d_1 = 1, 2, 5$ and 7 μm while d_2 was fixed at 5 μm. The temperature, pressure and number of periods are 90 K, 0 GPa and 10, respectively.

For d_2 in the range from 1 to 7 μm, the cutoff frequency varied approximately from 3.7 to 1.5 THz; while for d_1 in the same range, from 1 to 7 μm, the cutoff frequency barely changed from 0.8 to 2.1 THz. That is, it increased approximately only 1.3 THz, while in the case of the d_2 variation, it increased almost to a value close to 2.1 THz.

From these two responses, it can be noticed that the cutoff frequency is shifted in a higher amount due to modifications in the semiconductor layer than in the superconductor one.

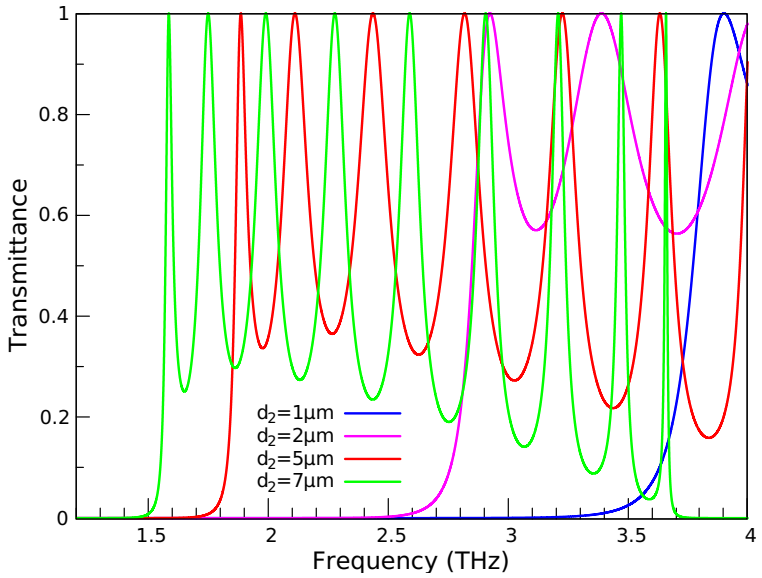


FIGURE 3.7: Cutoff frequency for $d_2 = 1, 2, 5$, and 7 μm while d_1 was fixed at 5 μm. The temperature, pressure and number of periods are 90 K, 0 GPa and 10, respectively.

3.3 Pressure dependence

In the Fig. 3.8 is presented the transmittance spectra for different values of the applied hydrostatic pressure. The values for the other quantities were $d_1 = 10$ μm, $d_2 = 5$ μm, $T = 90$ K and $N = 10$.

As the applied hydrostatic pressure increases, there are no noticeable changes in the cutoff frequency, but it can be noted that the width of the first gap increases slightly (from ~ 4 THz at 0 GPa to ~ 5 THz at 20 GPa), in addition to the the fact that the first two gaps are shifted to regions of higher frequency. The most notorious variation is presented in the region of 16–19 THz, where a new photonic band gap appears with the pressure increase.

It can also be seen in the overall behavior of the PC in Figs. 3.2, 3.4, 3.5 and 3.8 that the vertical cuts in the graphs are very sharp, therefore the superconductor-semiconductor PC can work as a very good frequency selector, as well as a band pass filter in the THz region; while for frequencies below the THz, it behaves like a good reflector.

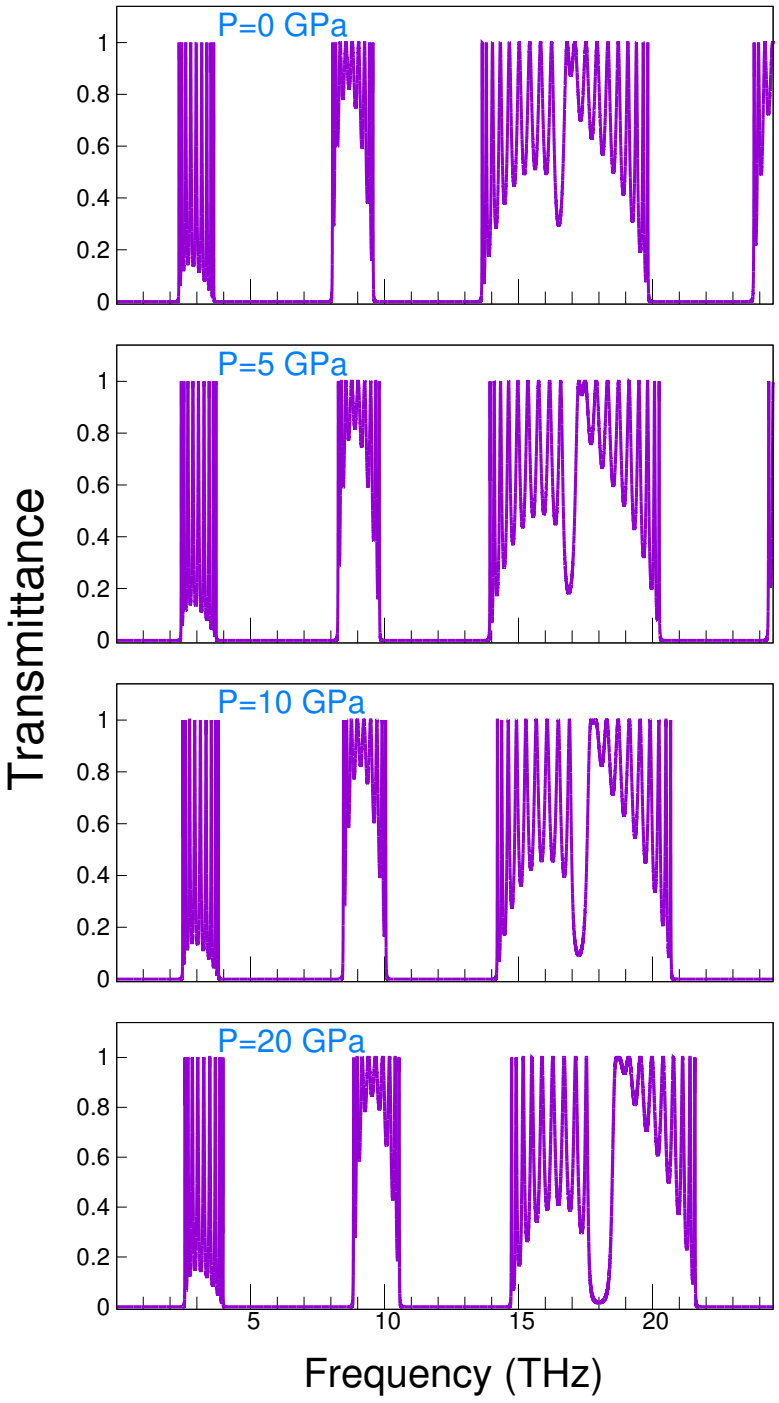


FIGURE 3.8: Transmittance spectra for different pressures with $d_1 = 10$ μm and $d_2 = 5$ μm. The number of periods and temperature are 10 and 90 K, respectively.

Chapter 4

Conclusions

Based on the results obtained in the project, as conclusions we state that:

- By using the transfer matrix method we have studied the transmittance properties of a one-dimensional superconductor – semiconductor photonic crystal.
- The cutoff frequency can be tuned by means of variations in the system temperature and thickness of the layers. As temperature as well as the semiconductor layer thickness are increased the cutoff frequency is decreased, whereas if the superconductor layer thickness is increased, so does the cutoff frequency.
- The cutoff frequency is shifted in higher amount by varying the thickness of the semiconductor layer than the thickness of the superconductor one.
- Also, we found that a hydrostatic pressure applied on the system can cause the appearance of a new photonic band gap, additionally to the fact that the width of the gaps vary.
- The vertical cuts in the graphs are very sharp, therefore the superconductor – semiconductor photonic crystal can work as a very good frequency selector, as well as a band-pass filter in the THz region.
- As a consequence of these results, we believe that a new series of experiments might be planned under these extreme pressure and temperature conditions, which could be used in communication systems.

Chapter 5

Outlook

As perspectives, in the future what is proposed is to add graphene layers to our previous structure, next to the semiconductor layers, and see how the system responses to spatial graphene features.

The reason to add graphene to the system is because of, as the superconductor material, graphene allows to tune the photonic band gaps by means of external parameters to the system, like temperature, or chemical potential through a gate voltage.

The idea is also to explore what is the response to a hydrostatic pressure applied in this new type of structures, subject which has not been studied so far.

Chapter 6

Conference presentations and publications

JOURNAL OF APPLIED PHYSICS **123**, 033101 (2018)

Pressure, temperature, and thickness dependence of transmittance in a 1D superconductor-semiconductor photonic crystal

Alan Y. Herrera,[a] J. M. Calero, and N. Porras-Montenegro
Departamento de Física, Universidad del Valle, A.A 25360 Cali, Colombia

(Received 19 October 2017; accepted 28 December 2017; published online 16 January 2018)

Using the transfer matrix method, we study the transmittance of 1D photonic crystals made of alternated layers of a semiconductor (GaAs) and a high-T_c superconductor ($HgBa_2Ca_2Cu_3O_{8+\delta}$) under the effects of temperature, applied hydrostatic pressure, and thickness of the layers. The frequency-dependent dispersion formula according to the two-fluid model was adopted to describe the optical response of the superconducting system. We found that increasing the superconductor (semiconductor) layer thickness results in a shift to higher (lower) values of the transmittance cut-off frequency. Additionally, this cutoff frequency is shifted to lower values with the temperature increase. Furthermore, we found that the width of the photonic bandgaps varies with the applied pressure. The most notorious variation is presented near the 17 THz region, where a new gap appears with the increase in pressure. We hope this work may be taken into consideration for the development of new perspectives in the design of new optical devices. *Published by AIP Publishing.* https://doi.org/10.1063/1.5009708



LA SOCIEDAD COLOMBIANA DE FÍSICA Y EL COMITÉ ORGANIZADOR DEL XXVII CONGRESO NACIONAL DE FÍSICA

CERTIFICA QUE:

PRESSURE, TEMPERATURE AND THICKNESS DEPENDENCE OF TRANSMITTANCE IN A 1D SUPERCONDUCTOR-SEMICONDUCTOR PHOTONIC CRYSTAL

Con autoría de ALAN YUSETH HERRERA FLOR, NELSON PORRAS MONTENEGRO, identificado con id 57 fue presentado bajo la Modalidad ORAL en el XXVII CONGRESO NACIONAL DE FÍSICA llevado a cabo en la Ciudad de Cartagena los días 3, 4, 5, 6 de Octubre de 2017.

CESAR TORRES MORENO
COORDINADOR ACADÉMICO

HERNANDO ARIZA CLADERÓN
PRESIDENTE DE LA SCF

XXVII Congreso Nacional de Física
Dirección General Universidad Popular del Cesar
Campus de Hurtado A: A: 590 Tel. 5843596 Valledupar
https://www.xxviicnf.com.co
contacto@xxviicnf.com.co

Financial Support

I would like to acknowledge financial support from Vicerrectoría de investigaciones at Universidad del Valle under grant No. (C.I) 71025.

Bibliography

[1] J. D. Joannopoulos, S. G. Johnson, J. N. Winn, and R. D. Meade. *Photonic Crystals: Molding the Flow of Light*. Princeton University Press (1995).

[2] E. Yablonovitch. *Phys. Rev. Lett.* **58**, 2059 (1987).

[3] S. John. *Phys. Rev. Lett.* **58**, 2486 (1987).

[4] A. H. Aly and D. Mohamed. *J. Supercond. Novel Magn.* **28**, 1699 (2015).

[5] S. Kazuaki. *Optical properties of photonic crystals*. Springer (2005).

[6] P. Lodahl, A. Floris van Driel, I. S. Nikolaev, A. Irman, K. Overgaag, D. Vanmaekelbergh, and W. L. Vos. *Nature* **430**, 654 (2004).

[7] S. Noda, M. Fujita, and T. Asano. *Nat. Photon.* **1**, 449 (2007).

[8] D. Mogilevtsev, S. Kilin, and S. B. Cavalcanti. *Photonics Nanostruct. Fundam. Appl.* **3**, 38 (2005).

[9] S. Noda, N. Yamamoto, M. Imada, I. Kobayashi, and M. Okano. *J. Lightwave Technol.* **17**, 1948 (1999).

[10] S. Noda, A. Chutinan, and M. Imada. *Nature* **407**, 608 (2000).

[11] S. John and T. Quang. *Phys. Rev. Lett.* **78**, 1888 (1997).

[12] H. Rauh and Y. A. Genenko. *J. Phys. Condens. Matter* **20**, 145203 (2008).

[13] C. H. Raymond and T. C. Yeung. *Phys. Lett. A.* **259**, 413 (1999).

[14] M. Tinkham. *Introduction to superconductivity, 2nd Ed.* McGraw-Hill (1996).

[15] L. E. Gonzales, J. E. Ordoez, M. E. Gomez, J. C. Granada, N. Porras-Montenegro, and G. Zambrano. yba$_2$cu$_3$o$_{7-x}$/ batio$_3$ one dimensional superconducting photonic crystal with tunable broadband response in visible region". , For Publishing.

[16] W. M. Lee, P. M. Hui, and D. Stroud. *Phys. Rev. B* **51**, 8364 (1995).

[17] A. Wall-Clarke and S. Savelév. *Phys. Rev. B* **85**, 214521 (2012).

[18] S. K. Srivastava and A. Aghajamali. *J. Supercond. Nov. Magn.* **30**, 343 (2017).

[19] A. H. Aly and W. Sabra. *J. Supercond. Novel Magn.* **29**, 1981 (2016).

[20] H.-M. Lee and J.-C. Wu. *J. Appl. Phys.* **107**, 09E149 (2010).

[21] A. H. Aly, S.-W. Ryu, H-T.. Hsu, and C.-J. Wu. *Mater. Chem. Phys.* **113**, 382 (2009).

[22] A. Macleod. *Thin-film optical filters*. CRC Press (2001).

[23] A. H. Aly, H.-T. Hsu, T-J.. Yang, C.-J. Wu, and C. K. Hwangbo. *J. Appl. Phys.* **105**, 083917 (2009).

[24] N. W. Ashcroft and N. D. Mermin. *Solid State Physics, 5th Ed.* Wiley, New York, 1976.

[25] M. Shur. *GaAs Devices and Circuits*. Springer US, 1987.

[26] L. E. Gonzáles and N. Porras-Montenegro. *Physica E* **44**, 773 (2012).

[27] J. B. Ketterson and S. N. S.N. Song. *Superconductivity*. Cambridge University Press (1999).

[28] R. Wesche. *Physical properties of high-temperature superconductors*. Wiley series (2015).

[29] A. Schilling, M. Cantoni, J. D. Guo, and H. R. Ott. *Nature* **363**, 56 (1993).

[30] A. Yamamoto, N. Takeshita, C. Terakura, and Y. Tokura. *Nature Communications* **6**, 8990 (2015).

[31] N. Takeshita, A. Yamamoto, A. Iyo, and H. Eisaki. *J. Phys. Soc. Jpn.* **82**, 023711 (2013).

[32] L. Gao, Y. Y. Xue, Q. Chen, F. Xiong, R. L. Meng, D. Ramirez, C. Chu, J. H. Eggert, and H. K. Mao. *Phys. Rev. B* **50**, 4260 (1994).

[33] P. Markos and C. M. Soukoulis. *Wave propagation: From Electrons to Photonic Crystals and Left-Handed Materials*. Princeton University Press (2008).

[34] G. A. Samara. *Phys. Rev. B.* **27**, 3494 (1983).

[35] A. M. Elabsy. *Phys. Scr.* **48**, 376 (1993).

[36] N. Porras-Montenegro and C. A. Duque. *Physica E.* **42**, 1865 (2010).

[37] R. I. Cottam and G. A. Saunders. *J. Phys. C: Solid State Phys.* **6**, 2105 (1973).

[38] C. H. Raymond, T. C. Yeung, C. H. Kam, and T. K Lim. *Phys. Rev. B* **61**, 5920 (2000).

[39] C. Panagopoulos, J. R. Cooper, G. B. Peacock, I. Gameson, P. P. Edwards, W. Schmidbauer, and J. W. Hodby. *Phys. Rev. B* **53**, R2999 (1996).

[40] B. F. Diaz-Valencia and J. M. Calero. *Physica C* **505**, 74 (2014).

[41] B. A. Hunter, J. D. Jorgensen, J. L. Wagner, P. G. Radaelli, D. G. Hinks, H. Shaked, Hitterman R. L., and R. B. Dreele. *Physica C.* **221**, 1 (1994).

[42] A. H. Aly, W. Sabra, and H. A. Elsayed. *J. Supercond. Nov. Magn.* **26**, 553 (2013).

[43] M.-S. Chen, C.-J. Wu, and T.-J. Yang. *Appl. Phys. A* **104**, 913 (2011).

[44] G. T. Jeong, J. I. Kye, S. H. Chun, S. Lee, S. I. Lee, and Z. G. Khim. *Phys. Rev. B* **49**, 15416 (1994).